Δελτίο της Ελληνικής Γεωλογικής Εταιρίας, Τομ. XXXIV/4, 1587-1594, 2001 Bulletin of the Geological Society of Greece, Vol. XXXIV/4, 1587-1594, 2001
Πρακτικά 9ου Διεθνούς Συνεδρίου, Αθήνα, Σεπτέμβριος 2001 Proceedings of the 9th International Congress, Athens, September 2001

DEFORMATION IN NISYROS VOLCANO (GREECE) USING DIFFERENTIAL RADAR INTERFEROMETRY

IS. PARCHARIDIS[1] & E. LAGIOS[1]

ABSTRACT

Nisyros Volcano located at the southeastern Aegean Sea (Greece) has recently shown (1996-97) a high seismic activity, associated with a significant deformation has determined by DGPS measurements. The determination of the overall deformation of the island was also attempted by Differential Radar Interferometry (DInSAR). The DInSAR analysis has been applied using the ERS-2 satellite data, covering the period 1996-1999. The removal of the interferometric phase related to the topography has been done using an external high resolution DEM. Two areas of the island show a good coherence, the southwestern and the eastern part. Almost two interferometric fringes were respectively recognized and evaluated. These two zones coincide with the main tectonic fractures of the island. The time separation and resolution, which consist important factors, for the extraction of the effective information and the quality of the finally produced differential interferogram, seem however that influence very slight its accuracy. The deformation outlined by the interferogram is compatible with the existing differential GPS observations.

KEY WORDS: Space Application, Differential Interferometry SAR, Volcanic Deformation, Nisyros Island (Greece).

1. INTRODUCTION

Volcano monitoring involves a variety of measurements and observations designed to detect changes at the surface of a volcano that reflect increasing pressure and stresses caused by the movement of magma, or molten rock, within or beneath it. An eruption occurs when magma rises from its source or from a storage reservoir and finally reaches the Earth's surface. As it rises, the magma fractures overlying rocks and parts of the volcano deform as magma is approaching the surface and makes space for itself.

There are three primary sources of crustal deformation at volcanoes: (i) pressure changes in high-level magma storage areas and conduits, (ii) magmatic intrusions and (iii) earthquakes. The most common model to interpret crustal deformation caused by pressure changes in high-level magma chambers is the Mogi model (Mogi 1958). Deformation associated with earthquakes and dike intrusions is not to be calculated using the Mogi model. For such deformation Okada (1985) presented a model, which can easily implemented in a computer.

There is a number of different geodetic techniques to monitor crustal deformation with different results of accuracy, the most important of which are: (i) Levelling, (ii) Tilt, (iii) Electronic Distance Measurements (EDM), (iv) Strain and (v) Global Positioning System (GPS).

In the last decade, Synthetic Aperture Radar (SAR) Interferometry has been proven to be a powerful technique for the generation of Digital Elevation Models and the monitoring of small surface changes on large-scale areas (Zebker and Goldstein 1986). Differential Interferometry (DInSAR) is the most interesting technique of SAR Interferometry in the two-dimensional mapping of deformation with very high accuracy (mm to cm level). The DInSAR technique allows the study of a wide range of surface deformations. Several applications mainly related to natural hazards could be carried out using DInSAR such as:

- Seismic risk and event management (Massonnet et al. 1993; Ponte 1997; Hanssen et al. 1996; Wright et al. 1999; Baer et al. 1999; Tramondo et al. 1999)
- Volcano monitoring (Wadge et al. 1997; Massonnet et al. 1997; Vadon and Sigmudsson 1997; Kobayashi et al. 1999)
- Subsidence risk (Avallone et al., 1999)

1. Space Applications Research Unit, Department of Geophysics-Geothermy, National and Kapodistrian University of Athens, Panepistimiopolis-Ilissia, Athens 157 84 (GR); e-mail: parchar@geol.uoa.gr, lagios@geol.uoa.gr

- Landslides (Fruneau et al. 1996; Redice et al. 2000).

In this paper we present preliminary results, obtained in the framework of Geowarn E.U Project (http:\www.geowarn.com), concerning the application of DInSAR technique to study the deformation at Nisyros volcanic island.

2. INTRODUCTION TO SAR DIFFERENTIAL INTERFEROMETRY

SAR interferometry measures the phase difference between two images of the same area taken on two different satellite passes (Fig. 1). This is generating the difference between the two phase-signals; then the phase-difference of any point on the ground will have a value ranging from 0 to 360. These phase-differences in the interferogram wrap around in cycles of 360 degrees and must be unwrapped to obtain the absolute phase. To successfully operate the interferometric process, a correlation must exist in the surface properties between the two image acquisitions. *Coherence* is a measure of the correlation between the two scenes used for the interferometric computation. This term is affected by the computation parameters, the perpendicular baseline (Bperp) and spatial changes (not displacement) – Fig. 1 -(Capes and Haynes 1996). The interferometric coher-

$$\gamma = \frac{\langle S_1 S_2^* \rangle}{\sqrt{\langle S_1 S_1^* \rangle \langle S_2 S_2^* \rangle}}$$

ence, γ, is defined as the normalized complex cross-correlation of both complex signals S_1 and S_2:

Where $\langle ... \rangle$ means the expectation value and * is the complex conjugation operator. The absolute value of the coherence varies from 0 (low coherence) to 1 (high coherence). The coherence depends on: (i) the baseline,

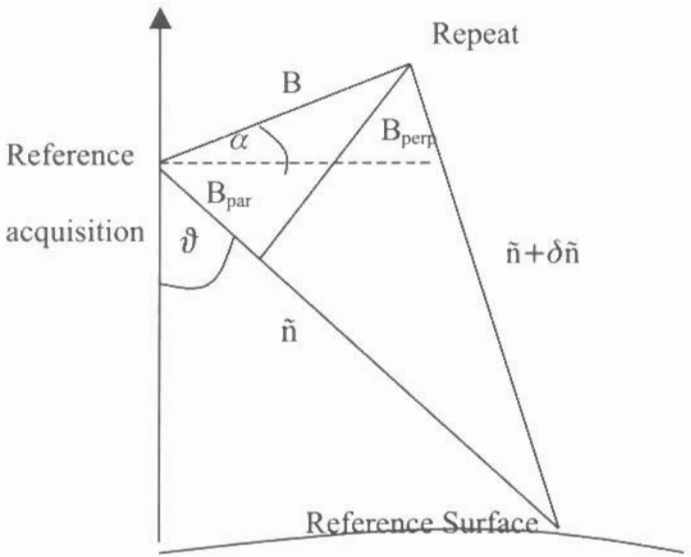

Figure 1. Geometry of the InSAR for a spheroidal Earth with no topography or deformation. B is the baseline length; B_{par} and B_{perp} are the components of the baseline parallel and perpendicular to the line of site, between the reference satellite and the ground (from Price and Sandwell, 1998).

(ii) the Doppler centroid and (iii) the additive noise on either signal or artifacts etc.

SAR interferometry (InSAR) is also used to estimate topographic heights. Differential interferometry (DInSAR) is the method to detect surface displacement events by subtracting a first interferogram representing the topography from a second interferogram representing the topography after the event causing the deformation (e.g. seismic event). Fringes related to common topography cancel each other, while the remaining fringes represent the changes in topography presenting the observed deformation.

The following equation describes the relation between the phase Ψ of the interferogram, the topographical

$$\Psi(P) - \Psi(P_0) = (4\pi/\lambda)\left\{\frac{B}{R\cdot\sin\theta}\Delta z + \delta r\right\}$$

elevation Δz and the surface change δr in the sland range:

Where P is a point and P_0 is a reference point, B is the baseline between the two orbits of the acquisition, R is the slant range to the P, and q is the incidental angle. Generally, the following different methods for differential interferometry are applied:

i. Three-pass Differential Interferometry
ii. Two-pass Differential Interferometry:
iii. Four-pass Differential Interferometry:

For detecting and measuring surface displacements, the following conditions should be considered:

- The SAR scenes should be spatially repeated as closely as possible, temporally and physically.
- The optimum baseline length (across-track separation) should be examined, between the two satellite positions, during the acquisition of the scenes (Zebker et al. 1994). The inaccuracy in the satellite orbit provides the ideal condition in interferometry; there are however limits to the baseline length. For surface changes, the baseline length estimate should be as short as possible (almost 0).
- The terrain changes, between the various satellite passes, should be examined because affect the phase information, such as:
- Systematic phase effects caused by large-scale motion taken place between the acquisitions (e.g. in cases of landslides).
- Phase effects caused by decorrelation of the phase contribution of scatters within the resolution cells, which means that the radar-scattering characteristics, within each pixel, must remain similar in the time between the passes. It is called temporal decorrelation, and it may be caused by rainfall, land use changes etc.
- Atmospheric effects (tropospheric and ionospheric) are another source of systematic error in surface displacement estimates deduced from SAR interferometry (Hansen and Feijt, 1996).

3. GEOLOGICAL SETTING

Nisyros is a strato-volcano at the southeastern end of the Hellenic Volcanic Arc (HVA) (Davis 1968; Di Paola 1974; Papanikolaou & Lekkas, 1990; Vougioukalakis 1993). The HVA is related to the northward subduction of the African Plate beneath the Aegean microplate. Most of the Nisyros Island is made of hyaloclastite, lava flows and breccias, mostly of andesite composition. Pyroclastic deposits and volcanic domes of dacite composition overlay these rocks.

The numerous thermal springs occurring mainly along the northern coasts and the emissions of gasses within the craters of the caldera, are the main volcanic activity of Nisyros during this century. According to Papanikolaou and Lekkas (1991), four main fracture zones dissecting the volcano in triangular segments are identified (see Fig. 1 in Lagios (2000)): (i) Zone F1 with direction NE-SW, (ii) Zone F2 with a direction NE-SW parallel to the previous one, (iii) Zone F3 with a direction NW-SE and (iv) Zone F4 that corresponds to a narrow graben with a direction of NNW-SSE.

In 1996, an earthquake activity started with earthquake magnitudes between M=4 and M=5 and continued up to May 1998. About 30 houses were damaged in Mandraki in July of 1996, due to the reactivation of an older fault, passing through the former little town. The scientific interest, relating to volcano monitoring observational techniques, such as the establishment of a GPS network, remeasured at least once per year (Lagios et al. 1998; Lagios 2000), yielding the deformation at the GPS stations was attracted by this seismic activity. However, the study of ground deformation at a much larger scale is now feasible, through the DInSAR technique, which is the main object of the present paper.

4. METHODOLOGY

Suitable interferometric pairs of SAR images have been selected after searching European's Space Agency FRINGE database to satisfy the technical parameters, such as the baseline and temporal separation. For selecting suitable data the following criteria have been used:

(i) Bp < 100 m
(ii) SAR acquisitions of the same season to avoid seasonal land use changes
(iii) Temporal separation including the period 1996 to 1997 (maximum of seismic activity).

Unfortunately only two SLC images were available (Table 1) with the appropriate baseline

length and temporal separation. From these two interferometric pairs only the second one was processed (Fig. 2). After the inspection of the leader file, at the first interferogram, was found that the Cross track Doppler frequency terms were of very high value (a value of 3724.097 Hz for the master scene, rather than a more expected value of 237.996 Hz for the slave scene). Therefore, the only one suitable interferometric pair, which was left for analysis, was the second one (Table 1). The Meteorological conditions for this interferogram (precipitations, moisture of the air, wind) were also appropriate during the day of the acquisition, provided by the Hellenic Meteorological Service. The only technical risk was related to possible inadequate image coherence, mainly due to relatively long temporal separation (1120 days). The ambiguity height, which is the amount of elevation change that produces one topographic fringe (Massonnet and Rabaute 1993), is high in both pairs (Table 1). The higher the ambiguity height value, the lower the sensitivity to topography is.

Interferometric pair	Master orbit	Date	Slave orbit	Date	Elapsed time (days)	Bp	Altitude of Ambiguity
1	10482	22/4/97	20502	23/3/99	700	-9	1046 m
2	5973	11/6/96	22005	6/7/99	1120	44	200 m

Table 1

The two-pass differential interferometry method (or DEM-elimination method) was applied. This method employs two SAR images, producing thus one interferogram. To perform the differential one, another interferogram has to be created or synthesized. The synthesized interferogram is generated from an existing digital elevation model (DEM). The synthesized interferogram is then subtracted from the original interferogram, thereby removing all fringes that relate to ground elevation, leaving only fringes that represent surface displacements. The phase differences that remain as fringes in the differential interferogram are a result of range changes of any displaced point on the ground from one interferogram to the next. In the differential interferogram, each fringe is directly related to the radar wavelength (56 mm for ERS satellites) and represents a displacement relative to the satellite of only half the above wavelength (28 mm).

The main steps of the interferometric processing include:

- External DEM production.
- Coregistration analysis to validate the input master/slave interferometric pair for spatial and spectral overlap.
- Coregister the external DEM to Master at a sub-pixel level accuracy.
- Interferogram generation. Range and azimuth spectral filtering should be applied to reduce the decorrelation of baseline and azimuth spectral shift. Flat Earth phase and optionally topographic phase should also be subtracted.
- Phase-coherence imagery generation for evaluating the quality of interferogram for phase unwrapping and random changes of land surface.
- Interferogram phase unwrap using up-to-date algorithms.

The above processing generates two InSAR geocoded images for the production of a differential interferogram for deformation estimates. The differential interferogram (change map) and the coherence imagery will be analyzed.

5. DATA PROCESSING

The differential interferometric SAR processing and analyses were based on the Atlantis software. At first the DEM of the island was created with a resolution of 4m/pixel by digitizing the contour lines from the topographic 1:5,000 scale map. As a next step, the initial orbit state vectors have been taken from the Delft Institute (NL) for Earth-Oriented Space Research (DEOS) for both scenes. DEOS precise ERS-2 orbits are based on the DGM-E04 gravity field model and the SLR and OPR2 altimeter crossovers and normal points (Scharroo & Visser 1998). In the coregistration step the master (11-6-96) and slave scene (6-7-99) were validated; a coregistration refinement was also performed between the two scenes of bilinear polynomial order, and the orbit/Earth geometric analysis was calculated. The input master scene and the external DEM were coregistered by displayed the external DEM as a simulated SAR image by selecting 39 common control points. The finally obtained RMS of the co-registration was 0.81 in the column direction and 0.88 in the row direction. After the generation of a first (raw) interferogram, the flat Earth phase and topographic phase were subtracted. A phase coherence map was created and the raw interferogram was enhanced.

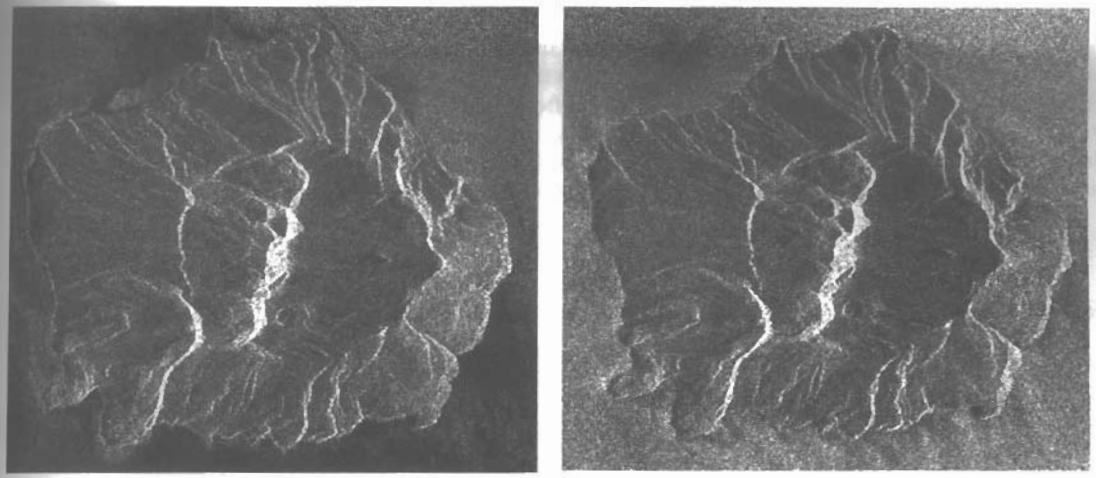

Figure 2. ERS–2 SLC subscenes of Nisyros Island. (a) Master-orbit N⁰ 5973 date 11-6-1996. (b) Slave-orbit N⁰ 22005, date 6-7-1999 (azimuth spectral overlap 98%).

Finally, the enhanced interferogram was unwrapped using the Disk Masking algorithm (EVInSAR Manual 1999). This method applies circular or elliptical disks centered on phase residues and pixels of low coherence. A number of unwrapping cycles have been performed, where the disks are enlarged in the first cycle, until no phase unwrapping discontinuity was detected. Furthermore, some unwrapping errors occurring in the low coherence areas were analyzed and repaired. The final differential interferometric image (Fig. 3) was a terrain corrected image and projected in latitude/longitude using the orbit/Earth geometry.

During the processing procedure, the data were checked step by step and the related information, like master and slave images spatial and spectral overlapping, baseline estimation, GCP's and RMS of the co-registration, were recorded in a text file for further elaboration.

6. QUALITATIVE AND QUANTITATIVE RESULTS EVALUATION

Almost 2 fringes in the western part of the island and two fringes in the southwestern part could be recognized in the final interferogram (Fig. 3). Every fringe is visualized as a cycle of gray levels intensities. The rest of the image is covered by "rumor" or fringes related to the topography. Generally, the differential image is highly depended on several factors, and as a consequence, the following should be considered in order to validate the results:

1. The quality of the DEM: A high resolution DEM was used, as described above.
2. The RMS error of the co-registration of the external DEM: A high number of co-registration tie-points have been used with an RMS error less than one pixel.
3. Quality of coherence: The temporal separation between the two acquisitions is relatively high (1120 days), which could favour the temporal decorrelation. It is deduced from the coherence image that the southwestern part of the island shows a fairly good coherence, the eastern part shows a medium coherence, while the coherence is low to very low at the rest of the island. The areas showing good coherence image correspond to Nikia rhyolites, Prophitis Helias dacites and lavas, while coherence is lost in the other rock-cover types, like pyroclastics, pumice etc. Additionally, the typical volcanic landscape of the island forms steep slopes in the caldera area, where the signal is not depicted by the satellite sensor (areas under shadow).
4. Possible atmospheric effects: Regarding effects due to changes in properties of the atmosphere, we can only rely on generalizations; ionospheric anomalies should be of small size and lower tropospheric effects will be related to weather or systematic change in moisture with height. This problem can be resolved by getting weather radar images for the same area, create more than one interferogram and/or obtain geodetic information. According to the Meteo Service, the weather was clear during the acquisition of the acquired scenes.

Regarding the qualitative evaluation of the final product, it represents a relatively homogeneous interferogram with a number of fringe patterns in the areas of actual deformation and noise phase in the other areas. The fringes in the southwestern and eastern part cannot be attributed to topography, because the relief from the coastline to the to edge of the [illegible] images are needed according

to the baseline, instead of the almost 2 presented in the interferogram. On the contrary, at the central southern portion of the area, where the coherence is low, the existing fringes could be attributed to the topography.

The most significant information, which confirms that the fringes are real and related to surface displacement is the existing Differential GPS data resulting from the remeasurement of the GPS network in Nisyros (Lagios et at. 1998). These observations show a relative deformation of 13mm to 37mm (average error estimate of less than 5mm) in the horizontal, and 14(+/-5) mm to 45(+/-10) mm in the vertical direction, during the period June-September 1997, which was even more increased to May 1998 (Lagios 2000).

Regarding the quantitative deformation, which is the estimation of the deformation towards the satellite within a few millimeters (28 mm for each fringe), the following considerations should be taken into account:

1. Large groups of pixels have been moved in different directions (this maintains the back-scattering characteristics of the area).

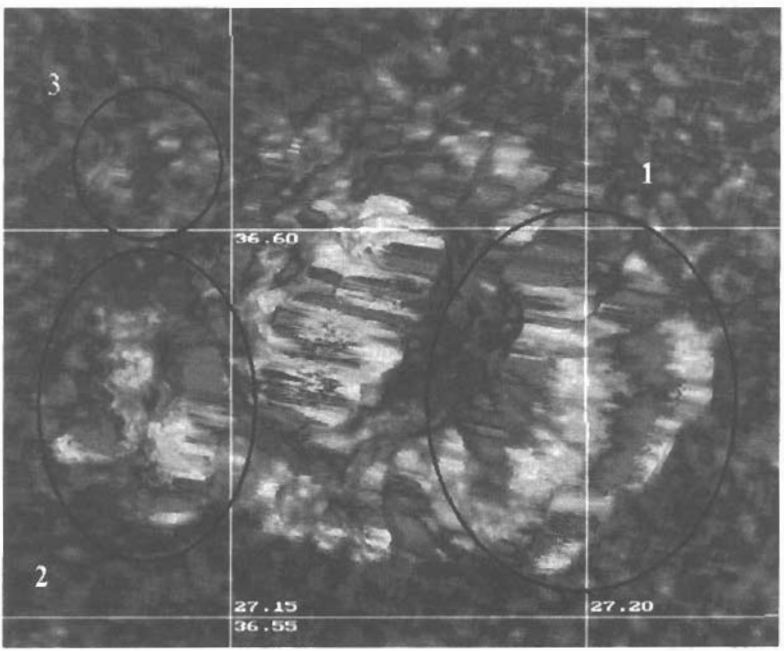

Figure 3. Differential Interferogram image (ERS-2, 11-6-96/6-7-99) of Nisyros Island (Magnitude & Phase). One fringe is visualized as a cycle of gray levels intensities.

2. Distinct fringe patterns are observed in areas of fairly good coherence. The areas 1 and 2 (Fig. 2), included in the black oval lines, correspond to fairly good coherence. The fringes in these areas correspond to surface displacement in the slant range, during the period of the dates of acquisition of the two scenes. In the area 1 (Nikia rhyolites), two non-completed fringes could be recognized, while in area 2 (Prophitis Helias dacites) there are two fringes. The two sites display different pattern of the fringe distribution and phase, which is increasing from the inner part to the outer of the island in both cases. The third oval line (Fig. 2), at the NW part of the island (corresponding to a medium to low coherence), shows one or two fringes. It is located in Mandrakion village, an area where the reactivation of an older known fault caused damages in buildings. There is, however in this case, an uncertainty to accept the marked fringes as actual deformation, due to the low coherence prevailing in that area.

It is very difficult to relate the deformation of the interferogram to vertical or horizontal movements using only the DInSAR data. Geodetic data (DGPS) and geological field observations are generally needed for comparison. After the confirmation of the type of displacement it should then be possible to define the quantity of the deformation. In the eastern part of the island the fringes follow the morphology, while the phase is increasing from the inner part to the outer. In the western part the fringes are less related to the morphology and the

phase is increasing from the inner to the outer part, meaning that in both cases the deformation is higher at the outer part. According to the Mogi's model, this happens in the case of horizontal movement for the first four kilometers in distance from the center of the volcano. Additionally, the eastern block seems to move towards east, and the western one towards southwest. The displacement could be quantified; each fringe represents 28 mm of displacement along the line of sight (the range direction) of the radar beam. The western therefore part would have been displaced about 60 mm, while the eastern part about 50 mm. These figures and the general picture of deformation resulting from the DInSAR analysis seem to be compatible with the DGPS observations (Lagios 2000) already existing in the island.

REFERENCES

AVALLONE, A., ZOLLO, A., BRIOLE, P., DELACOURT, C., BEAUDUCEL, F., 1999. Subsidence of Campi Flegrei (Italy) detecterd by SAR interferometry. *Geophysical Research Letters*, vol.26, No.15, p.2303-2306.

EVInSAR User's Guide 1999. Atlantis Scientific Inc.

BAER, G., SANDWELL D., WILLIAMS S. and BOCK Y. (1999). Coseismic deformation associated with the November 1995, Mw=7.1 Nuweida earthquake, Gulf of Elat (Agaba), detected by DInSAR. *J. Geophys. Res.* 104 (B11), 25221-25232.

CAPES, R. and HAYNES, M., 1996. A guide to SAR interferometry. Nigel Press Associates, Edenbridge, UK.

DAVIS E.N. 1967. Zur Geologie and Petrologie der Inseln Nisyros and Jali (Dodecanes). *Practika Acad. Athens*, 42, 235-252.

DI PAOLA, U., 1974. Volcanology and Petrology of Nisyros island (Dodecanne, Greece). Mem. Inst. Geol. Univ.Padova 7.

FRUNEAU, B., J. ACHACHE, and C. DELACOURT, 1996. Observation and modeling of the Saint-Etienne-de-Tinee landslide using SAR interferometry, *Tectonophysics*, 265 (3-4), 181-190.

HANSEN R. and FEIJT A., 1996. A first quantitative evaluation of atmospheric effects on SAR interferometry. Proceedings of Fringe'96 Workshop on ERS SAR Interferometry, Zurich, 30/9-2/10/96, 277-279.

KOBAYASHI S., FUJII N. & OKUBO S., 1999. Detection of Volcano deformations and co-seismic movements using JERS-1 L-band SAR differential Interferometry: Combination with other geodetic measurements. *Proceedings IGARSS'99*, II, 800-803.

LAGIOS, E., 2000. Intense crustal deformation rates on Nisyros Island (Greece), deduced from GPS studies, may foreshadow a forthcoming volcanic event. *Proc. 2nd Intern. Conf. On Earthquake Hazard and Seismic Risk Reduction*, 249-259.

LAGIOS E., CHAILAS S., GIANNOPOULOS J. & SOTIROPOULOS P., 1998. Surveillance of Nisyros Volcano: Establishment and remeasurement of GPS and Radon Networks. *Bull. Geol. Soc. Greece*, 32/4, 215-227.

MASSONNET, D & RABAUTE, T., 1993. Radar interferometry: Limits and potential, *IEEE Trans. Geosc. And Remote Sensing*, 31, 455-464.

MASSONNET, D., BRIOLE, P. and ARNAUD, A., 1995. Deflation of mount Etna monitored by spaceborne radar interferometry, *Nature*, 375, 567-570.

MASSONNET, D., ROSSI, M., CARMONA, C., ADRAGNA, F., PELTZER, G., FEIGL, K., & RABAUTE, T., 1993. The displacement field of the Landers earthquake mapped by radar interferometry, *Nature*, 364, 138-142.

MOGI, K., 1958. Relations between the eruptions of various volcanoes and the deformations of the ground surfaces around them. *Bull. Earthq. Res. Inst. Univ. Tokyo*, 36, 99-134.

PAPANIKOLAOU, D. and LEKKAS, E., 1990. Geological structure and evolution of the Nisyros Volcano. *Bull. Geol. Soc. Greece*, XXV/1, 405-419.

PELTZER, G. & ROSEN, P. (1995). Surface displacement of the 17 May 1993 Eureka Valley earthquake observed by SAR interferometry, *Science*, 268, 1333-1336.

PONTE S. (1997). ERS Tandem data for earthquake prediction: Preliminary results *Proc. 3rd ERS Symp. On Space at the service of our Environment*, Florence, Italy, 17-21 March 1997, ESA SP-414, 3, 499-506.

PRICE, E. J. and SANDWELL D. T., 1998. Small-scale deformations associated with the June 28, 1992, Landers, California, earthquake mapped by Synthetic Aperture Radar Interferometry phase gradients. *J. Geophys. Res.*, 103, 1-27.

REFICE A., BOVENGA F., WASOWSKI J. AND GUERRIERO (2000). Use of InSAR data for landslide monitoring: A case study from Southern Italy. *Proceedings IGARSS' 2000*, III, 2504-2506.

ROSEN, P., HENSLEY, S. & ZEBKER, H., 1996. Surface deformation and coherence measurements of Kilauea Volcano, Hawaii, from SIR-C radar interferometry, *J. Geophys. Res.* 101(E10), 23, 109-123, 148.

SCHARROO R. & VISSER P.N.A.M., 1998. Precise orbit determination and gravity field improvement for the ERS satellites, J. Geophys. Res., *103, C4, 8113-8127.*

TRAMONDO S., TESAURO M., BRIOLE P., SANSOSTI E., SALVI S., LANARI R., ANZIDEI M., BALDI P., FORNARO G., AVALLONE A., BUONGIORNO M.F., FRANCESCHETTI G. & BOSCHI E., 1999. The September 26, 1997 Colfiorito, Italy, earthquakes: Modeled co-seismic surface displacement from SAR Interferometry and GPS. *Geophys. Res. Lett.* 26(7): 883-886.

VADON, H., AND F. SIGMUNDSSON, 1997. Crustal deformation from 1992 to 1995 at the Mid-Atlantic ridge, southwest Iceland, mapped by satellite radar interferometry, *Science, 275* (5297), 193-197.

VOUGIOUKALAKIS G., 1993. Volcanic stratigraphy and evolution of Nisyros Island. *Bull. Geol. Soc. Greece,* 28/2, 239-258.

WADGE, G., ACHACHE, J., FERRETTI, A., FRANCIS, P.W., MORLEY, J., MULLER, J.P., Murray, J.B., PRATI, C., ROCCA, F., STEVENS, N.F., UPTON, M. & WILLIAMS, C.A., 1997. Volcano monitoring using Interferometric SAR. *Proc. 3rd ERS Symp. On Space at the service of our environment*, Florence, Italy, 17-21 March 1997, ESA SP-414, 3, 469-473.

WRIGHT T.J., PARSONS B.E., JACKSON J.A, HAYNES M., FIELDING E.J., ENGLAND P.C., CLARKE P.J. (1999). Source parameters of the October 1, 1995 Dinar (Turkey) earthquake from SAR interferometry and seismic bodywave modelling, *Earth and Planetary Science Letters*, 172, Issue 1-2, 23-37.

ZEBKER, H.A., & GOLDSTEIN, R.M., 1986. Topographic mapping from interferometric Synthetic Aperture Radar observations, *J. Geophys. Res.*, 91, 4993-4999.

ZEBKER, H.A., ROSEN, P.A., GOLDSTEIN, R.M, GABRIEL, A. and WERNER C.L., 1994. On the derivation of coseismic displacement fields using differential radar interferometry: the Landers earthquake. *J. Geophys. Res.*, 99, p. 19617-19634.